Biophysical Journal Volume 71 September 1996 1374–1388

Accelerated Interleaflet Transport of Phosphatidylcholine Molecules in Membranes Under Deformation

Robert M. Raphael and Richard E. Waugh
Department of Biophysics, School of Medicine and Dentistry, University of Rochester, Rochester, New York 14642 USA

ABSTRACT Biological membranes are lamellar structures composed of two leaflets capable of supporting different mechanical stresses. Stress differences between leaflets were generated during micromechanical experiments in which long thin tubes of lipid (tethers) were formed from the surfaces of giant phospholipid vesicles. A recent dynamic analysis of this experiment predicts the relaxation of local differences in leaflet stress by lateral slip between the leaflets. Differential stress may also relax by interleaflet transport of lipid molecules ("flip-flop"). In this report, we extend the former analysis to include interleaflet lipid transport. We show that transmembrane lipid flux will evidence itself as a linear increase in tether length with time after a step reduction in membrane tension. Multiple measurements were performed on 24 different vesicles composed of stearoyl-oleoyl-phosphatidylcholine plus 3% dinitrophenol-linked di-oleoyl-phosphatidylethanolamine. These tethers all exhibited a linear phase of growth with a mean value of the rate of interlayer permeation, $c_p = 0.009\ s^{-1}$. This corresponds to a half-time of ~8 min for mechanically driven interleaflet transport. This value is found to be consistent with longer times obtained for chemically driven transport if the lipids cross the membrane via transient, localized defects in the bilayer.

INTRODUCTION

The mechanical and thermodynamic properties of biological membranes are of considerable importance for proper cell function. However, the complexity of the membrane of even the simplest cell makes it difficult to achieve a detailed understanding of its properties. Consequently, a substantial part of research efforts in this field over the past 15 years has been directed toward understanding the properties of the phospholipid bilayer, the fundamental structural unit of all biological membranes. Many cellular processes, such as endocytosis and cell fusion, involve mechanical deformation and, in particular, changes in membrane curvature. Thus, the physical properties of bilayer membranes, especially those related to changes in curvature, are of fundamental interest in cellular biology.

The resistance of a membrane to changes in curvature is characterized by its bending rigidity. Recently, attention has focused on the subtle but important feature that the bending rigidity of a bilayer membrane is actually composed of two parts. There is an intrinsic stiffness of each monolayer to changes in curvature, giving rise to a localized resistance to bending that is characterized in terms of the local bending stiffness (or curvature elastic modulus), k_c (Helfrich, 1973). In addition, there is a resistance to bending a bilayer membrane that arises from the fact that when a bilayer membrane bends, the molecules in each layer are subjected to different strains. For an outward curvature, this results in an expansion of the outer leaflet of the bilayer and a compression of the inner leaflet. The molecules of the adjacent leaflets of the bilayer are not connected, which means that the molecules of the two leaflets may be redistributed independently to relieve different strains in the two leaflets. Therefore, this contribution to the bending energy is referred to as the "nonlocal bending energy" or the "global curvature energy" (Evans, 1974).

Qualitative aspects of the relationship between nonlocal bending elasticity and membrane shape were popularized by Sheetz and Singer (1974) in their "bilayer couple" hypothesis. This relationship was further explored by Svetina and Žekš (1989) and by Seifert et al. (1991), who made quantitative predictions about shape transformations in vesicles under the constraint that the area difference between two leaflets remained constant. Recently, Miao et al. (1994) have relaxed this constraint and instead used the form of the nonlocal bending energy introduced by Evans (1974) to predict the effect "area-difference elasticity" has on bilayer vesicle shape transformations.

Methods for assessing nonlocal bending elasticity in membranes are currently limited to a single technique, bilayer tether formation. This approach involves the formation of a thin tube of phospholipid bilayer (tether) from a large vesicle. Tether formation was first observed by Hochmuth et al. (1973), who formed tethers from the membranes of red blood cells in a flow channel. Since then, a number of new methods for forming tethers have been developed. These include the use of a second vesicle in a micropipette to pull tethers from a phospholipid vesicle (Evans and Yeung, 1994), the use of optical tweezers to pull tethers from neuronal growth cone membranes (Dai and Sheetz, 1995; Hochmuth et al., 1996), the use of glass fibers to pull tethers from red blood cells (Waugh and Bauserman, 1995), and the use of magnetic beads to pull tethers from phospholipid vesicles (Heinrich and Waugh, 1996). All of these techniques for applying and measuring forces on the order

Received for publication 8 December 1995 and in final form 6 June 1996.
Address reprint requests to Dr. Robert M. Raphael, c/o Richard E. Waugh, Department of Biophysics, University of Rochester School of Medicine and Dentistry, 601 Elmwood Ave., Rochester, NY 14642. Tel.: 716-275-3768; Fax: 716-275-6007; E-mail: rewaug@rbb1.biophysics.rochester.edu.

0006-3495/96/09/1374/15 $2.00

of 5 to 60 pN have increased our understanding of bilayer and cell mechanical properties.

The formation of a tether from a large vesicle produces an abrupt change in membrane curvature at the tether-vesicle junction. Thus, the work of tether formation includes a contribution due to the elastic energy required to bend the membrane. In addition, there is a contribution to the work that results from an expansion of the outer leaflet and compression of the inner leaflet of the vesicle as more material is drawn onto the outer than the inner leaflet as the tether length increases. This is the so-called nonlocal bending energy (Božič et al., 1992). The area difference between the leaflets ($\Delta A = A_{out} - A_{in}$) is related to the length of the tether (L_t) by

$$\Delta A = 2\pi h L_t, \tag{1}$$

where h is the separation distance between the neutral surfaces of the two monolayers. This relation reveals that tether formation is an extremely sensitive technique: a tether of length 60 μm formed from a vesicle with a surface area of 1000 μm^2 will result in a difference in leaflet area of 1.0×10^{-8} cm^2, corresponding to a difference in the number of lipid molecules in each leaflet of only 0.1%. Measurements of the change in equilibrium conditions with increasing tether length provided the first estimate of the magnitude of the nonlocal bending rigidity, designated k_r (Waugh et al., 1992).

These studies set the stage for investigating the dynamic features of bilayer deformation during tether formation, the subject of this report. The formation of a tether from a phospholipid vesicle produces an instantaneous, localized difference in mechanical stress supported by the two leaflets of the bilayer. This stress difference corresponds to a difference in area per molecule in the adjacent leaflets at the site where the tether is formed. Two mechanisms work to relieve this difference. One is the propagation of the difference over the vesicle surface by the lateral movement of the locally expanded outer leaflet relative to the locally compressed inner leaflet. The second is the relaxation of stress differences by the transmembrane movement of molecules from the compressed inner leaflet to the expanded outer leaflet (interlayer permeation or "flip-flop"). These two mechanisms are illustrated in Fig. 1.

The frictional interaction between the membrane leaflets as they slip past each other has been considered in detail by Evans and co-workers (Merkel et al., 1989; Evans et al., 1992; Evans and Yeung, 1994). They have proposed that the sliding of the layers past each other is limited by drag at the interface between the leaflets and have treated this "epitactic coupling" in terms of a simple, linear model. This impedance to relative motion is referred to as interleaflet drag and is characterized in terms of a coefficient, denoted b, which relates the relative velocity between the leaflets to the shear traction exerted by one leaflet on the other. Recently, Evans and Yeung (1994) have used tether formation

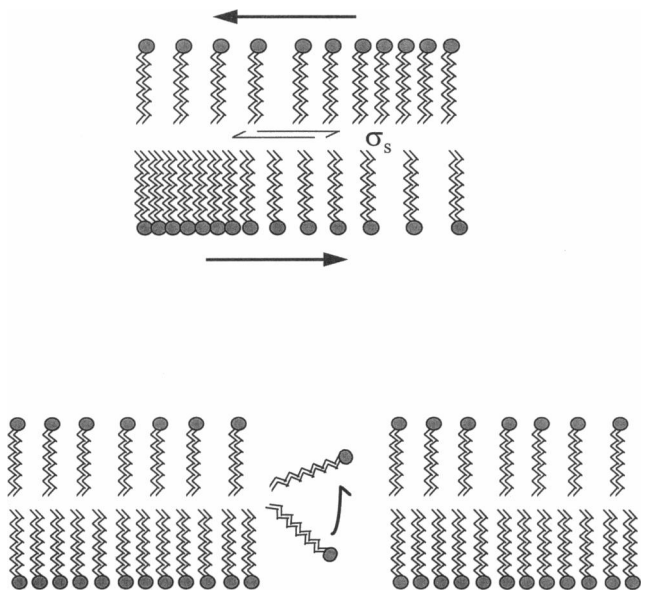

FIGURE 1 Two mechanisms for relaxing differential density in membranes. (*Top*) The leaflets slide relative to each other to equilibrate the area per molecule over the surface. This motion is opposed by the interlayer shear stress. (*Bottom*) Molecules move from the compressed leaflet to the expanded leaflet.

to measure the interlayer drag coefficient. Using a second vesicle as a force transducer and pulling out the tether at a constant velocity, they obtained values for b of $\sim 1.0 \times 10^8$ $N \cdot s/m^3$.

In the present study, a slightly different protocol is used in which a tether is formed from a vesicle via the weight of an attached glass bead. The tether is first held at equilibrium and then is subjected to a small step reduction in the aspiration pressure holding the vesicle in the pipette. Considering only interleaflet slip and not allowing for "flip-flop," a previous mechanical analysis led to the prediction that the tether should grow exponentially to a new equilibrium length (Evans et al., 1992). Examination of the tether formation process after a step change in pressure revealed that an additional slower dynamic process occurs during tether formation. Contrary to the predictions of previously published models, the response of the tether is biphasic, with an initial exponential relaxation (attributable to interlayer drag) plus a second linear phase of tether growth. The linear phase is consistent with the movement of molecules from the compressed inner leaflet of the bilayer to the outer leaflet to relax the differential tension in the membrane. As will be shown, the experimental results are consistent with the hypothesis that differential stretch in the membrane can drive the transport of molecules from one leaflet of the bilayer to the other. In this report we present both an extended mechanical analysis and experimental results of this novel method for measuring the rate of interlayer permeation (c_p) in membranes subjected to mechanical deformation.

MATERIALS AND METHODS

Vesicle preparation

The vesicles used in this study were formed by the method of Reeves and Dowben (1969), as modified by Needham and Evans (1988). The lipids 1-stearoyl-2-oleoyl-sn-glycero-3-phosphocholine (SOPC) and 1,2-dioleoyl-sn-glycero-3-phosphoethanolamine-*N*-[2,4-dinitrophenyl] (PE-DNP) were purchased from Avanti Polar Lipids. They were diluted to a concentration of 1.0 mg/ml in a 2:1 mixture of chloroform/methanol. The mixtures contained SOPC plus 3% PE-DNP and were stored under nitrogen at 4°C. The day before the experiment, the mixture was sonicated for 10 min, and then approximately 30 μl was removed and placed on the roughened surface of a teflon disc in a 50-ml beaker and dried in a vacuum for 2–3 h. A solution of 100 mM sucrose was then added and the vesicles were allowed to sit undisturbed overnight. In later experiments, the vesicles were shaken gently for 2 h on the day of the experiment.

Coating of glass beads with antibody

Glass beads (10–30 μm) were purchased from Polysciences (Warrington, PA). To improve the adhesion of the beads to vesicles, the beads were coated with an antibody to dinitrophenol (Molecular Probes, Eugene, OR). The procedure for coating beads was similar to that used for preparing an antibody matrix for immunoaffinity purification (Harlow and Lane, 1988). The beads were first mixed in a solution of acetone and silane and rocked gently overnight at room temperature. The beads were dried, washed, and then placed in a solution of 25% glutaraldehyde (EM grade) and shaken overnight at 37°C. The beads were washed again in a 0.5 M phosphate buffer and rocked overnight with the antibody. The next day, the beads were transferred to a solution of 100 mM ethanolamine to block any free reactive aldehyde groups.

The density of the glass beads was determined by measuring the settling velocity of approximately 30 beads as described previously (Bo and Waugh, 1989). The value of the density was determined to be 2.2 g/cm^3.

Microscope and optics

The experiments were performed on a microscope oriented so that the optical axis was horizontal. The vesicles were viewed through a 10× Hoffman modulation contrast lens. The optical signal was split and sent to two television cameras (RCA) to allow for a high-magnification and a low-magnification image. The entire experiment was recorded on videotape and played back for later analysis.

Procedure of experiment

The experiment involved the use of two separate chambers and three micropipettes, as illustrated in Fig. 2. The first pipette, the vesicle pipette, was used to aspirate vesicle and was connected via a continuous water-filled pathway to a water manometer used to control the aspiration pressure. A pressure transducer recorded the difference in pressure between the reservoir connected to the pipette and a reference reservoir. A second pipette, the reference pipette, was connected to a second transducer and was connected to the same reference reservoir as the vesicle pipette. Before the measurements, the zero pressure was adjusted in the vesicle pipette and the reference pipette by adjusting the reservoir height to the level at which no flow was observed. The movement of a particle in the reference pipette was used to detect and correct for any changes in the zero pressure in the chamber due to changes in the shape or height of the meniscus at the chamber entrance. Thus, this dual-pipette system allowed for accurate measurement of the aspiration pressure during the entire course of the experiment.

The vesicle chamber was used for storing and selecting the vesicles. The second chamber, the experimental chamber, was used for forming the tether. A third pipette, the transfer pipette, was used to transfer the vesicle and the pipettes from the vesicle chamber to the experimental chamber. The experimental chamber contained the glass beads, resting on a sanded-out "ledge" (see Fig. 2). This experimental chamber was formed by cementing a thin plastic coverslip cut to the desired dimensions to the plexiglass. The thinness of this lower part of the chamber helped reduce convection of the suspending fluid, thus providing a stable fluid environment in which to form tethers.

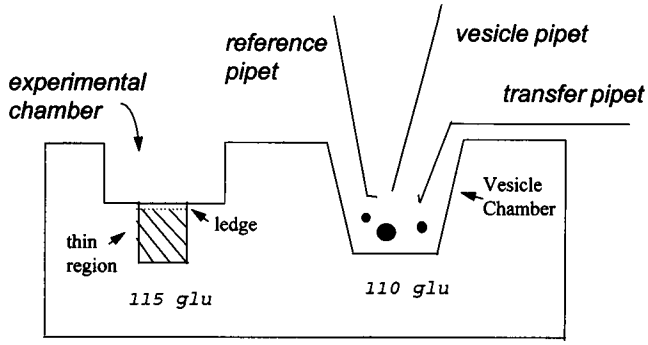

FIGURE 2 The experimental design. Vesicles were stored in a chamber containing 110 mM glucose. A single, thin-walled vesicle was selected and aspirated into a micropipette, which was then inserted into a larger transfer pipette. The chamber was lowered and moved sideways, and then the three pipettes were reinserted into the experimental chamber. The vesicle pipette was removed from the transfer pipette and the vesicle was manipulated to the ledge and attached to a glass bead. The vesicle-bead pair was then moved into the thin region of the chamber, and a tether was formed by reducing the aspiration pressure in the pipette. A particle was aspirated into the reference pipette to detect and correct any changes in the external pressure in the chamber.

At the beginning of the experiment, a few drops of the vesicle suspension were placed into the vesicle chamber containing 110 mM glucose plus 0.03% bovine serum albumin. (In later experiments 3.0 mM NaCl was added to this solution to facilitate adhesion of the vesicle with the glass bead.) A suitable vesicle was selected and aspirated into the vesicle pipette, which was then placed in the larger transfer pipette (diameter 75–125 μm). The vesicle was then transferred to the experimental chamber, which contained 115 mM glucose to further dehydrate the vesicle and produce a long projection of the vesicle into the pipette. The vesicle was then manipulated to the "ledge" and placed in contact with a glass bead. If adhesion was successful, the vesicle-bead pair was moved to the lower, thin region of the experimental chamber, and the pressure in the pipette was gradually reduced until the bead fell away from the vesicle, forming a tether. A schematic of the experiment is presented in Fig. 3.

To study the dynamics of tether formation, the pressure was adjusted to hold a very short tether at an equilibrium length for 5 to 15 min. Then a step change was made in the pressure and the growth of the tether was recorded as it traversed the field of view of the television camera. The pressure was then increased to return the bead to equilibrium at a short tether length, so that the process could be repeated. The experiments were performed at room temperature, with hydrated air blown into the experimental area to retard evaporation at the meniscus.

Accurate measurement of pipette diameters

Micropipettes were made from glass capillaries by first pulling the glass to fine needles on a pipette puller (Sachs Flaming Micropipette Puller, model PC-84; Sachs, Novato, CA). To break the end off cleanly, the pipette was inserted into a heated glass bead (a microforge). When the microforge current was turned off, the bead cooled and contracted, fracturing off the tip of the capillary and forming a smooth-tipped pipette. The inside diameters of the pipettes used in the experiments ranged from 6.7 to 9.2 μm.

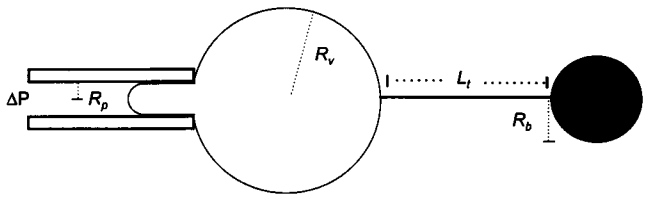

FIGURE 3 Schematic with variables used in the analysis. A giant phospholipid vesicle (15–30 μm in diameter) was aspirated into a micropipette forming a spherical outer portion of radius R_v and a projection into the pipette of length L_p. The vesicle was attached to a glass bead which, as it fell away from the vesicle, pulled out a tether of length L_t and radius R_t. The aspiration pressure in the pipette determines the tension in the membrane according to the law of Laplace (Eq. 5). The radius of the tether is not directly measurable but can be calculated from the change in the length of the vesicle projection in the pipette with changing tether length (cf. Eq. 19).

The error in the calculated parameters is subject to errors in the radius of the pipette (see Appendix B). Therefore it was desirable to achieve a very accurate measurement of the inner diameter of the pipette. Direct measurements from the video screen are limited by the diffraction pattern from the glass and were only accurate to approximately 0.5 μm. Therefore, to improve measurement accuracy, glass needles were coated with gold, and the diameter of the needle as a function of its length was accurately measured using scanning electron microscopy. The distance to which the probe could be inserted into the pipette was measured, and the inner diameter of the pipette was calculated from the known relationship between the probe length and the probe diameter. Using this approach, the inner diameter could be determined to an accuracy of 0.1 μm.

ANALYSIS AND CALCULATIONS

Tether equilibrium

The equilibrium analysis of the tether experiment has been performed from the standpoint of the elastic energy by Božič et al. (1992) and from the force balance approach in the work of Yeung (1994). The result is that at equilibrium, the tether force f is balanced by the isotropic membrane tension in the vesicle τ_o and the nonlocal bending contribution arising from the differential expansion and compression in the membrane ($\alpha_\pm$):

$$f = 2\pi\sqrt{2k_c\tau_o} + \frac{2\pi k_t}{h}\alpha_\pm. \tag{2}$$

The tether force f comes from the gravitational force on the glass bead and is essentially constant. The tension in the membrane at equilibrium, τ_o, can be calculated from the aspiration pressure in the pipette (ΔP_o) by applying the law of Laplace (Hochmuth and Evans, 1982):

$$\tau_o \approx \frac{\Delta P_o R_{v,o} R_p}{2(R_{v,o} - R_p)}. \tag{3}$$

Here R_p is the radius of the pipette, $R_{v,o}$ is the radius of the vesicle at the initial equilibrium state, and ΔP_o is the difference in pressure between the inside of the pipette and the external solution. The approximation sign indicates that the small contribution the force makes to τ_o has been neglected (Hochmuth and Evans, 1982).

The differential dilation field, $\alpha_\pm$, is related to the differential expansion/compression of the two leaflets of the bilayer caused by tether formation and is defined as $\alpha_\pm = \alpha_+ - \alpha_-$, where α_+ is the area strain for the outer leaflet resulting from a tension τ_+ and α_- is the strain for the inner leaflet resulting from a tension τ_-. In the simplest (equilibrium) case, in which there are no gradients in leaflet dilation over the vesicle surface, and in which the number of molecules in each leaflet is constant, the area difference between leaflets generated by formation of the tether (Eq. 1) results in a difference in the area per molecule over the vesicle surface. As the tether gets longer, the outer leaflet of the bilayer becomes more expanded while the inner leaflet becomes more compressed. Thus, in the tether experiment at equilibrium, the differential dilation $\alpha_\pm$ is related to the tether length L_t:

$$\alpha_\pm = \alpha_{o,i} + \frac{2\pi h L_t}{A_o}, \tag{4}$$

where A_o is the area of the vesicle. The parameter $\alpha_{o,i}$ is the initial or reference differential dilation and is introduced to account for the possibility that at zero tether length $\alpha_\pm$ may not be zero.

To study tether dynamics, a step change was then made in the aspiration pressure to initiate tether growth. The new tension in the membrane during the pulling process, τ_p, is calculated as

$$\tau_p \approx \frac{\Delta P_p R_{vav} R_p}{2(R_{vav} - R_p)}. \tag{5}$$

Here ΔP_p is the pressure during the pull and R_{vav} is the radius of the vesicle at the midpoint of the pull. R_{vav} was calculated from $R_{v,o}$ and changes in the projection length L_p via the condition that the area and volume of the vesicle were constant during the pulling process (described in Waugh et al., 1992).

The differential density imposed at the tether sphere junction is denoted α_o and can be calculated by applying the force balance equation before and during the pull. The resulting equation used to determine α_o is

$$\alpha_o = \alpha_{o,i} + h\frac{\sqrt{2k_c\tau_o} - \sqrt{2k_c\tau_p}}{k_t}. \tag{6}$$

Tether dynamics: the distribution of $\alpha_\pm$ on a sphere

The general equation governing the kinematic behavior of an axisymmetric bilayer membrane in which gradients in interleaflet stress differences exist or are being produced in

the bilayer was originally given by Evans et al. (1992):

$$\frac{\partial \alpha_{\pm}}{\partial t} = D_m \nabla_s^2 \alpha_{\pm} - c_p \alpha_{\pm}, \tag{7}$$

where ∇_s^2 is the Laplacian operator and c_p is a coefficient characterizing the rate of interlayer molecular transport. The coefficient of mechanical diffusivity, D_m, is proportional to ratio of the elastic compressibility modulus of the membrane, K, to the interlayer drag coefficient, b ($D_m = K/4b$). The coefficient b is formally defined as the proportionality constant between the interlayer shear stress (σ_s) and the corresponding difference between the velocities of the inner and outer leaflet, $v_{\pm}$:

$$\sigma_s = b v_{\pm}. \tag{8}$$

The units of b are N · s/m^3 (or dyn · s/cm^3). This first-order model for viscous drag between membrane leaflets was used in previous estimates of this parameter (Merkel et al., 1989).

The governing equation (Eq. 7) was solved by Evans and Yeung (1994) for the special case in which $c_p = 0$. The boundary condition for the problem is that the value of $\alpha_{\pm}$ at the tether-sphere junction is a constant. The initial condition is that the value of $\alpha_{\pm}$ at other points on the surface of the vesicle is zero. The solution for the time evolution of $\alpha_{\pm}$ on the surface of a spherical vesicle is expressed as an infinite sum of nonintegral Legendre polynomials:

$$\alpha'_{\pm}(\theta, t) = \alpha_o \left[1 - \sum_{s=0}^{\infty} A_s P_{\nu_s}(\zeta) e^{-\frac{\nu_s(\nu_s+1)D_m t}{R_v^2}} \right], \tag{9}$$

where α_o is the initial (constant) value of $\alpha_{\pm}$ at the boundary, and the prime indicates that we have taken $c_p = 0$. P_{ν_s} are Legendre functions with index ν_s and are functions of the angle $\zeta = \cos\theta$. The numerical values of ν_s are chosen to satisfy the boundary condition that the value of $\alpha_{\pm}$ remains constant at the boundary. Formulas for calculating these coefficients have been derived by Hall (1949). The coefficients A_s are calculated from the orthogonality property of the Legendre polynomials. Note that at long times the system is expected to attain a new equilibrium in which the differential dilation field at every point on the vesicle matches the value at the tether-vesicle junction.

Experimental observations of tether formation after a step change in the aspiration pressure were inconsistent with this prediction. Tethers were observed to grow at a constant rate beyond the expected equilibrium, consistent with a transport of molecules from the compressed inner to the expanded outer leaflet. We proceeded to solve the conservation equation, allowing for interlayer permeation. The solution to Eq. 7 allowing for interlayer transport (that is, nonzero c_p) can be obtained from the previous solution by a method due to Danckwerts (1951). If α' is the solution to the diffusion equation for the case in which $c_p = 0$, the solution for the case in which interleaflet lipid transport occurs is given by

$$\alpha_{\pm} = c_p \int_0^t \alpha' e^{-c_p t'} dt' + \alpha' e^{-c_p t}. \tag{10}$$

This method is valid when both functions have a constant value at the boundary and are zero at other points on the surface initially. Substitution of Eq. 9 for α' and integration yields

$$\alpha_{\pm}(\theta, t) = \alpha_o \left[1 - \sum_{s=0}^{\infty} A_s P_{\nu_s}(\zeta) \left(\frac{k_s e^{-(k_s + c_p)t} + c_p}{k_s + c_p} \right) \right], \tag{11}$$

where

$$k_s = \frac{D_m \nu_s(\nu_s + 1)}{R_v^2}.$$

Exponential terms for the index $s > 1$ decay rapidly, and the essential behavior of the system is contained in the first term of the sum. It is instructive to compare the complete solution for $\alpha_{\pm}$ as given by Eq. 9 or by Eq. 11 both at short and at long times. A plot of this solution at successive short time intervals is shown in Fig. 4. The horizontal axis is the value of the azimuthal angle θ, in radians, the tether being located at $\theta = \pi$. The vertical axis is the value of $\alpha_{\pm}$ normalized with respect to the value of $\alpha_{\pm}$ at the boundary. This figure was generated by solving for the first nonintegral Legendre coefficient ν_o and for the first expansion coefficient A_o, according to the formulas presented in Hall (1949). The coefficient of mechanical diffusivity D_m is on the order of 5×10^{-6} cm^2/s (Evans and Yeung, 1994), and R_v was taken to be 8 μm. The solid lines represent the solution to Eq. 9 and the dashed lines represent the solution

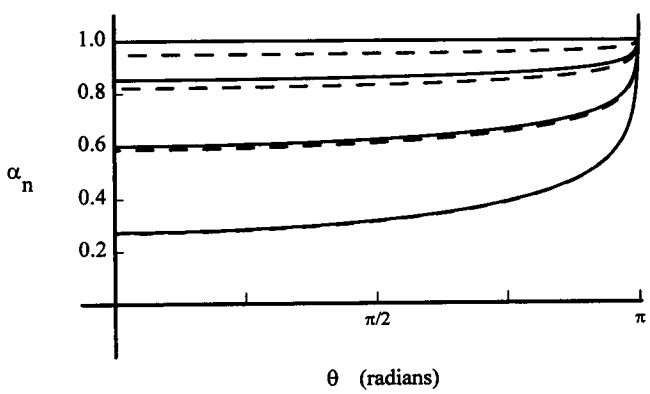

FIGURE 4 The spatial variation in $\alpha_{\pm}$ at successive time intervals. The vertical axis represents the value of $\alpha_{\pm}$ normalized with respect to the value of $\alpha_{\pm}$ at the boundary ($\alpha_n = \alpha_{\pm}/\alpha_o$). The horizontal axis shows the value of the angle θ, in radians, with the tether located at $\theta = \pi$. The solid line represents the solution without interlayer permeation, and the dashed line represents the solution with interlayer permeation. The pairs of curves (from bottom to top) correspond to the times $t = 2$ s, $t = 5$ s, $t = 10$ s, and $t = 120$ s. The curves were created from the approximate solutions given in Eqs. 9 and 11.

to Eq. 11, with $c_p = 0.01\ s^{-1}$. The successive curves (from bottom to top) are the distribution of $\alpha_\pm$ over the surface of the vesicle at the time points $t = 2$ s, $t = 5$ s, $t = 10$ s, and $t = 120$ s. As can be seen, the inclusion of interlayer permeation does not affect the solution much until about 10 s after the step change in membrane tension. (Note that the analysis by Evans and Yeung completely neglected interlayer permeation. Because their experiments were done on a time scale of 2 s, they were completely justified in dropping this term, even with our measured value of c_p.) Studies of the complete solution also show the justification for dropping higher order terms. Except at time 0, solutions carried out to one or 35 terms are indistinguishable.

Stress relaxation after tether recovery

The process of tether formation can be reversed. When the tether length reached the end of the field of view (or when the projection length in the pipette approached zero), the aspiration pressure was increased to pull the tether back to a short equilibrium length, so that the experiment could be repeated. After the tether returns to the vesicle body, the differential dilation built up during the growth phase requires that the tension needed to maintain a constant tether length be larger than was required before the pull. (During the pull, molecules move to relax $\alpha_\pm$ such that the tether length at which $\alpha_\pm$ is zero becomes larger. When the tether length is returned to zero, the increased number of molecules in the outer leaflet results in a compressive stress in the outer leaflet, that is, a negative $\alpha_\pm$. See Eq. 2.) As this residual $\alpha_\pm$ relaxes, the tension must be adjusted (reduced) to prevent the tether from returning to the vesicle.

As shown in Appendix A, there are two temporal phases to the relaxation of the system under these conditions. The initial phase is dominated by the rapid relaxation of gradients in $\alpha_\pm$ to make $\alpha_\pm$ uniform over the surface. This is followed by a slower relaxation as $\alpha_\pm$ goes to zero because of the transbilayer movement of lipids. It is shown in Appendix A that spatial variations in $\alpha_\pm(\theta, t)$ are rapidly dissipated when there is no flux of $\alpha_\pm$. Essentially, the conservation equation reduces to the form in which $\alpha_\pm$ is uniformly distributed over the surface, and the only mechanism available for the relaxation is transbilayer movement of lipid molecules. The relaxation of differential dilation will be related to the rate of interlayer permeation by

$$\frac{\partial \alpha_\pm}{\partial t} = -c_p \alpha_\pm. \tag{12}$$

To a good approximation, the solution is given by a simple exponential decay:

$$\alpha_\pm(\theta, t) = \alpha_\pm(\theta, 0) e^{-c_p t}, \tag{13}$$

where $\alpha_\pm(\theta, 0)$ is the initial value of the differential density on the sphere at the time the tether reached a short length ($t = 0$). Hence, the dilation field will decay through transbilayer movement of phospholipid molecules to zero if enough time is allowed.

From the force balance, we know the value of $\alpha_\pm(\theta_o, t)$ at any time t. If we assume this second part of the return phase proceeds through a series of quasi-equilibrium states, with spatial variations being rapidly dissipated (Appendix A), the prediction is that the square root of the membrane tension will decay exponentially while the tether is held at the short equilibrium length:

$$\sqrt{\tau(t)} = \frac{1}{\sqrt{2k_c}} \left[\frac{f}{2\pi} - \alpha_{st} e^{-c_p t} \right], \tag{14}$$

where α_{st} is a constant resulting from the integration of the distribution of $\alpha_\pm$ over the surface of the vesicle immediately after the tether is returned (see Appendix A).

Calculation of b, c_p, and k_r from experimental time course

The general solution to the time evolution of the differential density field, including interlayer permeation, is given in Eq. 11. When this solution is applied to our experimental method of tether formation, a prediction for the time course of tether formation in terms of three unknown variables, b, c_p and k_r, is obtained (see Appendix A). The theoretical prediction for the time course of tether formation is given by

$$L_t(t) = L_{t,o} + \frac{2R_v^2 \alpha_o}{h(1 + c_p(t_d + t_b))^2} \left[1 - e^{-\left(\frac{1}{t_d + t_b} + c_p\right) t} \right] + c_p \frac{2R_v^2 \alpha_o}{h(1 + c_p(t_d + t_b))} t. \tag{15}$$

Measurements of the tether length as a function of time were fit to the sum of an exponential and linear time course, via nonlinear least-squares regression (Levenberg-Marquardt algorithm, Origin; Microcal Software, Northampton, MA). The form of the fitting equation was

$$L_t(t) = L_{t,o} + L_{tint}(1 - e^{-t_{exp} \cdot t}) + V_{tav} \cdot t, \tag{16}$$

where $L_{t,o}$ is the initial measured length of the tether and the other three experimental parameters are determined from the fit: L_{tint} (the length the tether that would have been obtained in the absence of the linear growth term), t_{exp} (the time constant of the exponential phase), and V_{tav} (the velocity of the linear phase of tether growth).

By comparing these two equations, we see that the experimental parameters can be related to the material parameters by algebraic relations. We then arrive at a system of three equations in three unknowns, which can be solved by substitution. The solution of this system results in the following equations used to calculate the membrane material

constants:

$$c_p = t_{exp}\frac{V_{tav}}{L_{tint}\cdot t_{exp} + V_{tav}}, \tag{17a}$$

$$k_r = t_{exp}^2 \cdot R \cdot X_3 \frac{L_{tint}}{L_{tint}^2 \cdot t_{exp}^2 + 2\cdot L_{tint}\cdot t_{exp}\cdot V_{tav} + V_{tav}^2}, \tag{17b}$$

$$b = -\{X_2 \cdot L_{tint}^2 \cdot t_{exp}^2 + 2\cdot X_2 \cdot L_{tint}\cdot t_{exp}\cdot V_{tav} + X_2 \cdot V_{tav}^2 - t_{exp}\cdot R\cdot X_3 \cdot L_{tint} - R\cdot X_3 \cdot V_{tav}\} \cdot [X_1 \cdot (L_{tint}^2 \cdot t_{exp}^2 + 2\cdot L_{tint}\cdot t_{exp}\cdot V_{tav} + V_{tav}^2)]^{-1}, \tag{17c}$$

where the following definitions were employed:

$$R = \frac{2R_v^2}{h}$$

$$X_1 = 2h^2R_v^2\ln(R_v/R_t)$$

$$X_2 = 6\mu R_b R_v^2 \tag{18}$$

$$X_3 = h(\sqrt{2\cdot k_c\tau_o} - \sqrt{2\cdot k_c\tau_p}).$$

The value of the monolayer separation distance, h, was taken to be 4 nm.

The radius of the tether, R_t, can be determined from conservation of area during the pulling process as described previously (Hochmuth and Evans, 1982; Bo and Waugh, 1989):

$$R_t = R_p\left(1 - \frac{R_p}{R_{vav}}\right)\left(-\frac{dL_p}{dL_t}\right). \tag{19}$$

This relation is valid only if the radius of the tether does not depend on its length. The linearity of the relationship between measured values of L_p and L_t confirmed that the tether radius was constant during the pulling process (see Fig. 5) and thus justified the use of Eq. 19. Occasionally vesicles did not show this linear relation, and those were not included in the data set.

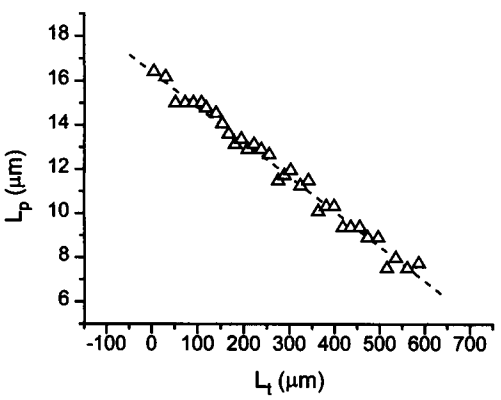

FIGURE 5 The relationship between the tether length (L_t) and the projection length in the pipette (L_p) during a pull. The dashed curve represents a linear regression to the measured values. The linearity of this relationship indicated that the tether radius was constant during the pulling process.

Calculation of k_c

The equations for calculating b, c_p, and k_r derived above contain k_c, the local bending rigidity, in the parameter X_3. It has been shown previously that tether formation provides a measurement of k_c from the balance of forces in the membrane at equilibrium (Bo and Waugh, 1989; Waugh et al., 1992). It is also possible to calculate k_c in our dynamic experiments by the relation (Evans et al., 1992)

$$k_c = 2\tau_p R_t^2. \tag{20}$$

Although R_t is usually quite well determined, the tension during the pull (τ_p) can have errors due to an error in the vesicle radius, pipette radius, or aspiration pressure measurement. Thus, this relation becomes especially inaccurate if the aspiration pressure during the pull is low. Therefore, to calculate the value of k_c, we have determined the expected uncertainty in each of the experiments. This was done based on an error propagation analysis presented in Appendix B. The data were then weighted by the their expected variance to produce an estimate for k_c according to the equation

$$\hat{k}_c = \frac{\sum(k_{c,i}/\sigma_{k_{c,i}}^2)}{\sum(1/\sigma_{k_{c,i}}^2)}, \tag{21}$$

where the sum is performed over i measurements and the variance of each measurement ($\sigma^2_{kc,i}$) is calculated as described in Appendix B. A 95% confidence interval for k_c is then $\hat{k}_c \pm 2\sigma_{kc}$.

RESULTS

Tether growth

The time course of tether formation after a step change in the membrane tension is shown in Fig. 6. Similar time courses have been measured for over 24 vesicles. The response is biphasic, with an initial exponential increase followed by a linear phase of tether growth (see Fig. 6). The raw data are fit to the form of Eq. 16. In general, the coefficient of determination of the fit was greater than 0.99, and the 95% confidence intervals for the fitted parameters were typically within 5% of their value. The theory predicts that the time course of tether formation should depend on the magnitude of the step change in the boundary tension. In Fig. 6, the results of an experiment in which multiple pulls were performed on the same vesicle are presented. In this particular example, the values of the change in membrane tension ($\Delta\tau$) were 0.011 mN/m, 0.027 mN/m, 0.034 mN/m, and 0.045 mN/m, and the corresponding values in L_{tint} were 16 μm, 117 μm, 133 μm, and 179 μm, respectively. The agreement between the experimental results and the theo-

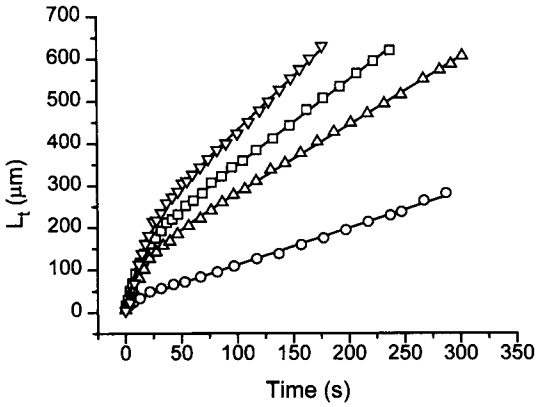

FIGURE 6 The time course of tether growth for multiple, increasing step changes in the membrane tension. The reductions in tension were 0.011 mN/m (○), 0.027 mN/m (△), 0.034 mN/m (□), and 0.045 mN/m (▽). Solid curves represent least squares-fits to the data according to Eq. 16. These data were obtained from a single vesicle in which a tether was formed repeatedly at different, constant values of the tension. Even for an extremely small change in the membrane tension, the tether continued to grow without an apparent approach to equilibrium. The tether growth rate was faster for larger step changes in the boundary tension, consistent with the hypothesis that differential density can drive transbilayer movement of molecules. (Note that 1 dyn/cm = 1 mN/m.)

retical predictions provides strong support for the analytical model of tether formation.

Data were obtained on over 24 vesicles, many of which were subjected to multiple pulls. A total of 64 "pulls" were performed. The estimated value of k_c obtained from these measurements according to Eq. 20 and weighted according to Eq. 21 was $k_c = 1.18 \times 10^{-19}$ J. Inasmuch as k_c is a material constant and should be the same for membranes of the same composition, this value of k_c was used in all subsequent calculations of membrane material properties. Histograms of the values of b, c_p, and k_r obtained from Eqs. 17a–17c are shown in Fig. 7. The mean (unweighted) calculated values of the parameters were $b = 4.5 \times 10^8$ N-s/m^3, $k_r = 3.7 \times 10^{-19}$ J, and $c_p = 0.009$ s^{-1}.

Dependence of rate of interlayer permeation on differential density

Examination of the data for a possible dependence of the rate of interlayer permeation on the magnitude of the membrane tension or the difference in membrane tension between leaflets is of interest because such a dependence might indicate that increases in differential stress have an effect on the permeability of the membrane for transbilayer movement of phospholipid molecules. In Fig. 8, the calculated value of c_p plotted as a function of α_o (the magnitude of the differential dilation at the boundary) is presented. As can be seen, there is no apparent correlation between these two parameters. Similarly, there was no dependence of c_p on the magnitude of the membrane tension for values of the

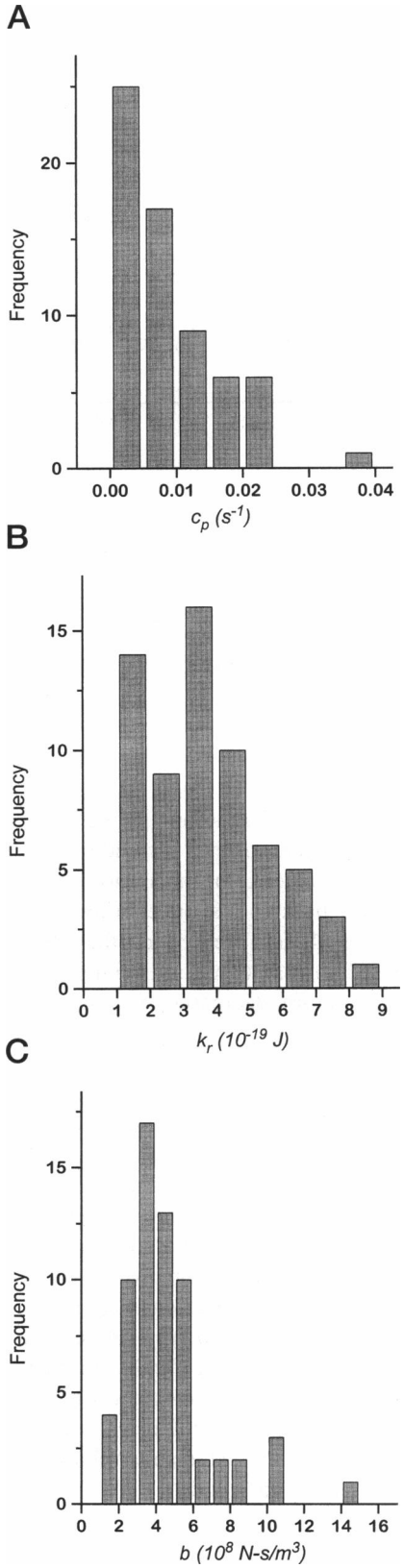

FIGURE 7 Histograms of the calculated material coefficients for 64 tether "pulls." (*A*) The calculated values of c_p. The mean value (± SD) was 0.009 (±0.007) s^{-1}. (*B*) The calculated values of k_r. The mean was 3.74×10^{-19} ($\pm 1.46 \times 10^{-19}$) J. (*C*) The calculated values of *B*. The mean was 4.57×10^8 ($\pm 2.38 \times 10^8$) N·s/m^3.

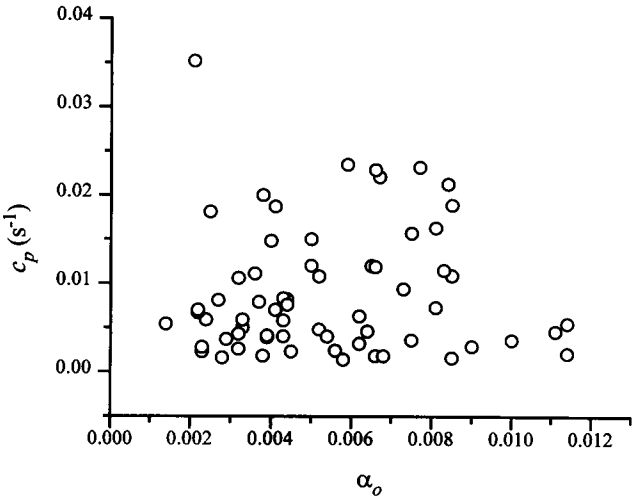

FIGURE 8 Calculated values of c_p as a function of α_o. The plot shows no correlation between the measured rate of interlayer permeation and the magnitude of the differential density (α_o), which is proportional to the difference in mechanical stress between leaflets.

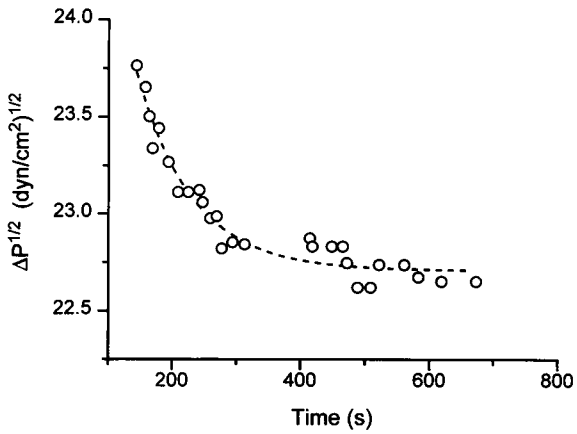

FIGURE 9 The time course of pressure relaxation at a fixed short tether length. After the tether reached the limit of view of the camera, it was pulled back by increasing the aspiration pressure. After the tether reached a very short length, the aspiration pressure was adjusted (reduced) to maintain a fixed short length. Circles indicate measured values. The dashed line shows least-squares regression for a simple exponential relaxation. The time constant for this relaxation is the coefficient of interlayer permeation. (Note that 10 dyn/cm^2 = 1 Pa.)

tension used in the present study, that is, up to 0.2 mN/m (data not shown).

Tether return

The process of tether formation can be reversed and repeated. When the tether reached the end of the field of view of the television camera, the aspiration pressure was increased to pull it back to a short equilibrium length. Consistent with the analytical predictions, the square root of the tension required to maintain equilibrium at a short tether length after its return decreased on an exponential time course (Fig. 9). Nonlinear least-squares regression using an exponential decay function revealed a time constant reflecting the coefficient of interlayer permeation, c_p (see Eq. 14). For this vesicle the time constant of the relaxation was 86 s, corresponding to a value of c_p of 0.0116 s^{-1}. In practice, it was often difficult to obtain precise data in this phase of the experiment, as the pressure was adjusted manually to maintain the short tether length, and a slight overadjustment of the pressure could greatly distort the curve. However, acceptable relaxation data were obtained in 35 cases. The average value of c_p calculated from these data is 0.011 $\pm$ 0.004 s^{-1}. In light of the difficulty in making reliable measurements of the relaxation of the membrane tension, the agreement between this value of c_p and the mean value of c_p calculated from the extensional phase of the experiment (0.009 s^{-1}) is quite good.

DISCUSSION

Interpretation of rate of dissipation of differential dilation

Bending a bilayer membrane in a localized region introduces differential density gradients between the adjacent leaflets. These gradients are expected to relax by distributing over the entire surface by a mechanically driven slip between the leaflets of the bilayer (Evans and Yeung, 1994). The most significant feature of the present work is the observation of an additional mechanism for dissipating differential density that is distinct from interlayer slip. This additional dissipation is attributable to the relaxation of stress differences between the membrane leaflets by the transbilayer movement of phospholipid molecules ("flip-flop").

The rate constant c_p measured in this study can be related to the half-time for transbilayer movement of phospholipids by equating a kinetic description with a nonequilibrium thermodynamic description of the system. Our measured value of c_p corresponds to a half-time for flip-flop of ~8 min. On first consideration it appears that this rate is inconsistent with the rates that have been measured previously in pure bilayer systems. The movement of phospholipids across the bilayer is expected to be slow. Measurements of the half-time for "flip-flop" of phosphatidylcholine molecules have ranged from 6 h (Kornberg and McConnell, 1971) to several days (Rothman and Dawidowicz, 1975). Other studies (Homan and Pownall, 1988; see Zachowski, 1993, for a review) have corroborated the consensus that passive transbilayer movement "does not occur on any reasonable time scale" (Yeagle, 1993).

How then do we reconcile our observations of rapid flip-flop with this consensus? Previous measurements of flip-flop have been made by introducing a probe molecule (fluorescent or spin-label) into one leaflet of the bilayer and measuring its rate of disappearance or reappearance on the opposite side of the membrane. Most of these measurements have been made in sonicated, small unilamellar vesicles (SUVs). One study has indicated that the rate of transbilayer

movement is faster in large unilamellar vesicles (LUVs), but the half-time for flip-flop in these vesicles is still on the order of 9 h (Wimley and Thompson, 1990), 100 times slower than the rate we have measured under conditions of mechanical stress.

A number of investigators have postulated that flip-flop occurs through localized defects in the membrane surface (Homan and Pownall, 1987; Wimley and Thompson, 1991; and Devaux, 1991). Wimley and Thompson based their conclusion on thermodynamic arguments and demonstrated that the hypothesis is consistent with measurements of proton transport, which is thought to occur via similar structures (Paula et al., 1996). Consideration of the rate-limiting steps in transbilayer movement via localized defects provides a way to reconcile the relatively rapid rate at which transmembrane stress differences relax with the much slower relaxation of transmembrane concentration differences. The activation energy for interleaflet transport by defects is attributed to the formation of the defect, and the barrier to transport of a molecule through the defect once it is formed is thought to be negligible. In this case, the transport of probe molecules across the bilayer is limited by the probability that a defect exists and the diffusive transport of the molecules laterally along the membrane to the defect site. Lateral diffusion of lipid is fast compared to the rate of transbilayer movement, so the occurrence of defects must be rare (Devaux, 1991).

Relaxation of mechanical stress via defects also depends on the probability of defect formation and the lateral transport of molecules to the defect. In this case, however, the lateral transport is driven by stress gradients in the membrane and limited by the drag between the leaflets as the two surfaces slide over each other in the vicinity of the defect. The governing equation for this process is derived from consideration of force balance and continuity, but it takes a form identical to that of the diffusion equation (Evans and Yeung, 1994), except that the characteristic coefficient is the mechanical diffusivity rather than the lateral diffusion coefficient (Eq. 7, with $c_p = 0$). The mechanical diffusivity has been determined by Evans and Yeung (1994) and by us to be $\sim 5 \times 10^{-6}$ cm^2/s, about 100 times larger than the lateral diffusion coefficient, $\sim 5 \times 10^{-8}$ cm^2/s (Wu et al., 1977). Thus, for a given probability of defect formation, mechanical stress gradients are expected to relax about 100 times faster than concentration differences.

It is important to emphasize that this explanation of accelerated interleaflet transport via defects is based on the increased rate of mechanically driven (rather than diffusion-driven) transport of material to the defect, not an increase in the frequency or lifetime of the defects themselves. This is in contrast to other situations in which defect formation has been invoked to explain instances of more rapid interleaflet lipid movements. For example, Wimley and Thompson (1990) argue that the rate of transbilayer movement observed in LUVs is more rapid than that observed in SUVs (Rothman and Dawidowicz, 1975), because the constraints on headgroup reorganization in SUVs reduce the probability of defect formation. Increased rates of flip-flop in vesicles near the phase transition temperature, or in membranes containing bilayer-perturbing elements (proteins or nonbilayer lipids), can also be attributed to an increase in the formation and persistence of defect structures (De Kruijff and Van Zoelen, 1978; De Kruijff et al., 1978; Homan and Pownall, 1988).

Experiments in which interleaflet transport is measured under conditions in which the surface geometry of the membrane is constrained may be more difficult to interpret. For example, Needham and Zhelev (1995) have measured the interleaflet transport of lysophosphatidylcholine (LPC) in micropipette aspirated vesicles and found a half-time for flip-flop of LPC of ~300 s, similar to what we have measured. In those experiments, however, multiple factors are likely to be involved. LPC should facilitate the formation of defects in the membrane, leading to increased transport rates, but in addition, stress differences between the leaflets are likely to result from preferential incorporation of LPC into the outer leaflet and the constraints on membrane geometry imposed by pipette aspiration. This could further increase the tendency toward defect formation, but could also accelerate the movement of lipids through a defect once it has formed.

Another situation in which stress-enhanced lipid flip may be important is in measurements of lipid asymmetry and transport in red blood cell membranes. In this case, the constraint on geometry resulting from the presence of the membrane skeleton, in combination with the incorporation of probe molecules or the transport of lipid via "flippases" to the outer membrane (Devaux and Zachowski, 1994), would be expected to produce small stress differences between the lipids of the opposing leaflets of the bilayer. These stresses would drive a nonspecific transport of lipids to the inner leaflet of the membrane. This mechanism could account for the nonspecific lipid transport pathway postulated by Brumen et al. (1993) to reconcile their observations and modeling of lipid transport and lipid asymmetry in red blood cells.

Measurement of nonlocal bending rigidity

The measured value of the nonlocal bending rigidity presented in this report, $k_r = 3.7 \times 10^{-19}$ J, is slightly lower than that reported previously by our laboratory, $k_r = 4.1 \times 10^{-19}$ J (Waugh et al., 1992). The present study has two advantages over the previous one. The more complete theoretical analysis and the curve-fitting method for the determination of k_r should provide a more accurate measure of this parameter. Second, the inclusion of the reference pipette enables us to make sure that the aspiration pressure remained constant during the experiment, which was an assumption that could not be verified formerly.

Measurement of interleaflet drag

The frictional interactions that occur between molecularly thin surfaces are an area of recent scientific interest (Bhushan et al., 1995; Yoshizawa et al., 1993; Yoshizawa and Israelachvili, 1994). Although less attention has been paid to the frictional interactions that can occur in biological membranes, these interactions can have important biological effects on the shape of a membrane and the dynamics of intracellular transport.

This report provides support for the model of Evans and Yeung (1994), that the dominant dynamic resistance to tether formation comes from viscosity between the leaflets of the bilayer as they slide past each other into the tether region. Evans and Yeung reported a value of b on the order of $\sim 1.0 \times 10^8$ N-s/m^3, whereas our measured value is $\sim 4.5 \times 10^8$ N-s/m^3. We note that the tether growth velocities in the experiment of Yeung were on the order of 100–400 μm/s, whereas ours were on the order of 1–5 μm/s. It is possible that the different values reflect a dependence of the interlayer drag on the slip velocity, but the difference might also be attributable to measurement error. Our ability to determine b is limited by Stokes drag on the bead. Furthermore, the expression for calculating b is expressed in terms of squares of the other parameters (Eq. 17c), resulting in a large expected uncertainty for b (see Appendix B). In light of these considerations, the value for b we have obtained agrees reasonably well with values reported previously (Evans and Yeung, 1994; Hochmuth et al., 1996).

As pointed out by Evans and Yeung (1994), this dynamic coupling between the monolayers gives rise to "hidden dynamics" during rapid changes of bilayer shape. Although not considered previously, interlayer drag will affect the interpretation of thermal fluctuations of bilayer vesicles (Yeung, 1994). Our results further indicate that moderately rapid dissipation of differential stress is also possible in situations of high curvature. This effect could be especially important in shape changes that involve "narrow" necks (Fourcade et al., 1994; Miao et al., 1994), such as budding and vesiculation.

CONCLUSION

The present results indicate that in situations involving membrane deformation and the generation of a driving force for lipid movement, gradients in local leaflet density can be dissipated by two mechanisms: one consistent with the lateral redistribution of the leaflets relative to each other, and the other consistent with the movement of phospholipid molecules from one leaflet to the other. The rate of interleaflet transport is much more rapid than expected, based on chemical probe measurements of lipid flip-flop. This accelerated transport can be rationalized if lipid movement between leaflets occurs at localized defects, because mechanically driven transport of molecules to the defect site is 100 times faster than lateral diffusion. Thus, in situations in which transmembrane stress differences may arise, the "conventional wisdom" that non-protein-mediated mechanisms for lipid transport can be neglected may be incorrect, and movement of lipids between bilayer leaflets may result in relatively rapid relaxation of stress differences.

APPENDIX A

Solution for rate of tether growth

The solution for the time evolution of the differential dilation field without interlayer permeation over the surface of the vesicle can be expressed as

$$\alpha'_{\pm}(\theta, t) \approx \alpha_o \left[1 - \frac{k e^{-(k+c_p)t} + c_p}{k + c_p} P_{v_o} \right], \qquad \text{(A1)}$$

where,

$$k = \frac{D_m v_o}{R_v^2} = \frac{D_m}{2R_v^2 \ln(R_v/R_t)},$$

and v_o is the first nonintegral value at which the corresponding Legendre polynomial P_{v_o} vanishes at the boundary. The higher order terms (Eq. 9 in the manuscript) have been neglected.

The task now is to relate this solution to experimentally measurable parameters in the tether experiment. We cannot directly measure $\alpha_{\pm}$, but we can calculate changes in this quantity from the balance of forces because changes in the force equilibrium are revealed by changes in the length of the tether. Hence, we need to solve for the rate of tether growth by matching the flux of material onto the tether to the tether velocity, V_t. This is done by applying the condition of incompressibility at the tether-sphere junction and matching the relative velocity to the diffusive flux (Yeung, 1994):

$$D_m \frac{\partial \alpha_{\pm}}{\partial s}\bigg|_{\theta_o} = v_{\pm} = \frac{h}{2R_t} V_t. \qquad \text{(A2)}$$

The expected rate of tether growth can be obtained from this relation and the solution for $\alpha_{\pm}$ presented above. However, there is a slight complication in our experiment, which is that the boundary condition is time-dependent. The boundary condition is set by the force, and in our experiment, the force is not constant, as it is complicated by Stokes drag on the glass bead. When this is included in the force balance equation, the boundary condition can be written as

$$\alpha(t) = \alpha_o - \frac{12\mu R_b}{hK} V_t, \qquad \text{(A3)}$$

where μ is the viscosity of water, R_b is the radius of the bead, h is the separation distance between the neutral surfaces of the bilayer, and K is the elastic compressibility modulus of the membrane.

The solution of problems with time-dependent boundary conditions can be obtained from the known solution for problems in which the boundary condition is time-independent by the use of Duhamel's theorem (convolution), discussed in Özisik (1968) and Carslaw and Jaeger (1959). If $\alpha_{\pm}(\theta, t) = \alpha_o \cdot g(\theta, t)$ is the solution for the time-independent boundary condition problem with $\alpha_{\pm}(\theta_o, t) = \alpha_o$, then the solution when the boundary condition is $\alpha(\theta_o, t) = \alpha(t)$ is

$$\alpha_{\pm}(\theta, t) = \int_0^t \alpha(\tau) \frac{\partial}{\partial t} g(\theta, t - \tau) d\tau. \qquad \text{(A4)}$$

Using the solution for $\alpha_\pm$ with interlayer permeation given in Eq. 11 in the manuscript and applying the flux boundary condition given in Eq. A2, we obtain (by the method of Laplace transforms) the theoretical prediction for the time course of tether formation:

$$L_t(t) = L_{t,o} + \frac{2R_v^2\alpha_o}{h(1 + c_p(t_d + t_b))^2}\left[1 - e^{-\left(\frac{1}{t_d + t_b} + c_p\right)t}\right] + c_p \frac{2R_v^2\alpha_o}{h(1 + c_p(t_d + t_b))}t, \tag{A5}$$

where α_o can be calculated from Eq. 6 and t_d and t_b are defined as

$$t_d = 2R_v^2 \ln(R_v/R_t)/D_m$$
$$t_b = \frac{6\mu R_b R_v^2}{k_r}. \tag{A6}$$

Solution for return problem

In the tether experiment, tether formation can be reversed by imposing a new tension that acts to restore the tether to the body of the vesicle. According to the force balance, this procedure is the same as introducing a new value of $\alpha_\pm$ at the vesicle-tether boundary (denoted α_r) at some time $t = 0$. The reverse problem begins with a nonzero distribution of $\alpha_\pm$ on the vesicle surface, which can be calculated exactly from the Eq. A1. However, if the experiment has reached steady state, $\alpha_\pm$ will be essentially constant over the surface of the vesicle, so we approximate the distribution as uniform with a value α_f. (This is accurate, except at a region very close to the junction, as shown in Fig. 4.) The solution for the differential dilation field during the reverse phase was obtained using a Laplace transform. It is given by

$$\alpha_\pm(\theta, t) = \alpha_r\left[1 - \sum_{s=0}^{\infty} A_s P_{v_s}\left(\frac{\alpha_r - \alpha_f}{\alpha_r} e^{-(k_s + c_p)t} - \frac{c_p e^{-(k_s + c_p)t} - c_p}{k_s + c_p}\right)\right]. \tag{A7}$$

Note that as t goes to infinity, $\alpha_\pm$ should approach the value set at the boundary α_r. In practice, however, this condition is not reached because the tether experiment is constrained by the condition that the tether length remain positive. Thus, when the tether length becomes small, the tension and hence the value of $\alpha_\pm$ at the boundary are adjusted to maintain constant tether length. In terms of $\alpha_\pm$ this means that the flux of $\alpha_\pm$ onto the vesicle at the boundary is constrained to be zero. There are two temporal phases to the relaxation of the system under these conditions. The initial phase is dominated by the rapid relaxation of gradients in $\alpha_\pm$ to make $\alpha_\pm$ uniform over the surface. This is followed by a slower relaxation as $\alpha_\pm$ goes to zero because of the transbilayer movement of lipids.

The mathematical statement of this problem is as follows. Defining $t = 0$ as the time when the tether has reached a short length, the initial condition is that $\alpha_\pm(\theta,0)$ is given by Eq. A7. The governing equation and the boundary conditions are

$$\frac{\partial \alpha_\pm}{\partial t} = D\nabla_s^2\alpha_\pm - c_p\alpha_\pm$$
$$\left.\frac{\partial \alpha_\pm}{\partial \theta}\right|_{\theta=\theta_0} = 0 \tag{A8}$$
$$\alpha_\pm(\theta, 0) = f'(\theta) \quad \text{for any } \theta \neq \theta_0,$$

where $f'(\theta)$ is given by the expression in Eq. A7, evaluated at the time when the tether has reached the short equilibrium length.

We solve this problem using the standard technique of separation of variables. To calculate the eigenvalues v_s, we use the boundary condition, which reduces to

$$\left.\frac{\partial P_{v_s}}{\partial \theta}\right|_{\theta=\theta_0} = 0. \tag{A9}$$

We recall that the Legendre polynomials can be expressed in terms of the hypergeometric function. Hence, to satisfy the boundary condition we must calculate the derivative of the hypergeometric function with respect to z. An expression for this derivative is given by Abramowitz and Stegun (1965, p. 557):

$$\frac{d}{dz}F[a, b; c; z] = \frac{ab}{c}F[1 + a, 1 + b; 1 + c; z]. \tag{A10}$$

The boundary condition requires that

$$v_s(1 - v_s)F[1 + v_s, 2 - v_s; 2; z_0] = 0. \tag{A11}$$

This equation is satisfied by the trivial results that $v_s = 0$ and $v_s = 1$ and by the zeroes of the hypergeometric equation. Thus, the prediction is that $\alpha_\pm$ will decay to zero with a time constant governed by the sum of k_s and c_p. The first zero is $v_o = 0$, and thus k_o is also zero. The value of the first nonintegral Legendre polynomial is 1 ($P_{vo} = 1$ for $v_o = 0$), and so the solution can be expressed as

$$\alpha_\pm(\theta, t) = \alpha_{st}A_o e^{-c_p t} + \alpha_{st}\sum_{s=1}^{\infty} A_s P_{v_s} e^{-(k_s + c_p)t}, \tag{A12}$$

where α_{st} is a constant term resulting from the integration of the nonuniform distribution ($f'(\theta)$) over the surface of the vesicle.

The value of v_1 is 1.0, and for a typical value of $D/R_v^2 = 2.34$, k_1 is 4.68 s^{-1}, meaning the time constant for the relaxation is approximately 0.2 s. The next higher order term yields a time constant of 0.07 s. Thus, the higher order terms decay rapidly and the solution for this part of the return phase can be written as

$$\alpha_\pm(\theta, t) \approx \alpha_{st}e^{-c_p t}. \tag{A13}$$

Note that this solution can be obtained by solving the conservation equation without the diffusive term. If we were to assume enough time has been allowed for $\alpha_\pm$ to be uniformly distributed over the surface, the only mechanism available for the relaxation is transbilayer movement of lipid molecules. The more complete analysis was performed to determine the time course of spatial variations in $\alpha_\pm$, and to ensure that such variations would decay sufficiently rapidly.

APPENDIX B: ERROR PROPAGATION ANALYSIS

The expressions for the calculation of the material parameters given in Eqs. 17a to 17c include different combinations of parameters obtained from the nonlinear least-squares regression fit to the measured time course of tether formation. In addition to the fitted parameters, the tether experiment requires the measurement of several other quantities, all of which are subject to uncertainty. The goal of the analysis in this appendix is to calculate the expected variability of the values of material constants that will be obtained in the tether experiment, given the uncertainty of the experimental parameters.

To accomplish this we use the principles of multivariate error analysis, also referred to as the delta method (Bevington, 1969; Clifford, 1973). This method enables the calculation of the expected uncertainty in a quantity when the uncertainty of each of the variables used to calculate that quantity and the partial derivatives of that quantity with respect to each of the

variables are known. In general, for a function $x(u,v,z)$, the variance of x (σ_x^2) can be expressed as

$$\sigma_x^2 = \mathbf{A}\,\mathbf{C}\,\mathbf{A}^T \tag{B1}$$

$$\mathbf{A} = \left(\frac{\partial x}{\partial u}, \frac{\partial x}{\partial v}, \frac{\partial x}{\partial z}\right),$$

where $\mathbf{A}^T$ denotes the transpose of $\mathbf{A}$, and $\mathbf{C}$ is the variance-covariance matrix, which has diagonal elements σ_{uu}^2, σ_{vv}^2, and σ_{zz}^2, which represent the variance in each of the variables. The uncertainty in the variables is the square root of the variance, which is commonly referred to as the standard deviation. In what follows, for each of the errors discussed, the reason for choosing a particular value of σ will be discussed. If the errors in u, v, and z are uncorrelated, the off-diagonal elements of the variance-covariance matrix are all zero. However, for parameters determined from nonlinear least-squares regression fits, the errors in the parameters are correlated, and therefore all of the elements of the variance-covariance matrix must be taken into account.

Expected deviation in k_c

The expected standard deviation in the calculated value of k_c can be obtained by writing the tension during the pull (τ_p) and the tether radius (R_t) in terms of the experimentally measured variables. Equation 20 then takes the form

$$k_c = \frac{(dL_p/dL_t)^2 P_p R_p^3 (R_{vav} - R_p)}{R_{vav}}, \tag{B2}$$

where dL_p/dL_t is the slope of the L_p versus L_t curve (Fig. 5), P_p is the pressure during the pull, R_p is the radius of the pipette, and R_{vav} is the average radius of the vesicle during the pull. The expected variance for k_c is obtained following Eq. B1:

$$\sigma_{k_c}^2 = \sigma_P^2\left(\frac{\partial k_c}{\partial P_p}\right)^2 + \sigma_{R_v}^2\left(\frac{\partial k_c}{\partial R_v}\right)^2 + \sigma_{R_p}^2\left(\frac{\partial k_c}{\partial R_p}\right)^2 + \sigma_{dL_p}^2\left(\frac{\partial k_c}{\partial dL_p}\right)^2. \tag{B3}$$

As evident from Eq. B3, the expected variance in k_c depends on the accuracy of the aspiration pressure, the accuracy of the vesicle radius, the accuracy of the pipette radius, and the accuracy in the slope of the L_p versus L_t curve. From consideration of the pixel size on the screen as well as making different measurements of the same vesicle, the uncertainty in R_v was taken to be ± 0.3 μm (i.e., $\sigma_{R_v} = 0.3$ μm). The pipette radius was determined by inserting a probe into a pipette, and the accuracy of its measurement was limited by the ability to resolve the probe diameter as a function of insertion distance. The uncertainty in the pipette radius was taken to be ± 0.1 μm ($\sigma_{R_p} = 0.1$ μm). The transducer that records the aspiration pressure was sensitive to changes in 0.1 mm H_2O (or 1.0 N/m^2), so the uncertainty in the aspiration pressure (σ_P) was taken to be 1.0 N/m^2. The accuracy of the slope of the L_p versus L_t curve (σ_{dL_p}) was taken to be the standard error of the linear regression fit. The expected uncertainty in k_c was generally on the order of 0.1 to 0.2 $\times$ 10^{-19} J, but could be as large as 0.7 $\times$ 10^{-19} J. Note that k_c can also be determined from the force balance (Eq. 2). An error propagation analysis of this equation revealed that an error in the bead radius propagated to a large error in the force and a less accurate determination of k_c. The expected uncertainty from the force relationship was generally three times larger than the expected uncertainty obtained by the tether radius relationship (Eq. 20).

Expected deviation in c_p

The expected standard deviation in the calculated value of c_p can be obtained by applying Eq. B1 to Eq. 17a. The resulting equation is

$$\sigma_{c_p}^2 = \sigma_{t_{exp}}^2\left(\frac{\partial c_p}{\partial t_{exp}}\right)^2 + \sigma_{L_{tint}}^2\left(\frac{\partial c_p}{\partial L_{tint}}\right)^2 + \sigma_{V_{tav}}^2\left(\frac{\partial c_p}{\partial V_{tav}}\right)^2 + 2\left(\frac{\partial c_p}{\partial L_{tint}}\right)\left(\frac{\partial c_p}{\partial t_{exp}}\right)\sigma_{t_{exp},L_{tint}} + 2\left(\frac{\partial c_p}{\partial L_{tint}}\right)\left(\frac{\partial c_p}{\partial V_{tav}}\right)\sigma_{L_{tint},V_{tav}} + 2\left(\frac{\partial c_p}{\partial_{t_{exp}}}\right)\left(\frac{\partial c_p}{\partial V_{tav}}\right)\sigma_{t_{exp},V_{tav}}. \tag{B4}$$

The last three terms arise from the correlation between the variables obtained from the nonlinear least-squares regression. The first three terms can be expressed as

$$\sigma_{c_p}^2 = \sigma_{t_{exp}}^2\frac{V_{tav}^2}{(L_{tint}\cdot t_{exp} + V_{tav})^2} + \sigma_{L_{tint}}^2\frac{L_{tint}\cdot t_{exp}}{(L_{tint}\cdot t_{exp} + V_{tav})^2} + \sigma_{V_{tav}}^2\frac{-t_{exp}\cdot V_{tav}^2}{(L_{tint}\cdot t_{exp} + V_{tav})^2} + \ldots, \tag{B5}$$

where the other three terms arising from the off-diagonal elements of the variance-covariance matrix have not been explicitly written down. Note that because c_p depends only on the parameters from the fit to the experimental time course, the uncertainty in c_p depends only on the uncertainty in these parameters ($\sigma_{L_{tint}}$, $\sigma_{t_{exp}}$, and $\sigma_{V_{tav}}$). The uncertainty in the parameters from the nonlinear least-squares regression fit was obtained from the variance-covariance matrix. For very good fits, the resulting error in c_p is on the order of 10%. When the fit is not very good, the expected error in c_p can be as large as 50%.

Expected deviation in k_r

The expected uncertainty in the calculated value of k_r can be obtained by applying Eq. B1 to Eq. 17b. In addition to depending on the three parameters from the fit, the error in k_r depends on the error in the variables R and X_3, which are functions of experimentally measured variables R_v (the vesicle radius) and τ_o and τ_p (the tension in the membrane before and during the pull). The tension in the membrane depends on three parameters: the radius of the vesicle, the radius of the pipette, and the measured value of the aspiration pressure. The expected uncertainty in these parameters has been discussed above. From these values, the expected standard deviation of the membrane tension was calculated by the delta method. This uncertainty was then used to determine the uncertainty in X_3. The results indicated that, even for a good fit, the uncertainty in k_r can be as high as 30%.

Expected deviation in b

The expected deviation in the calculated value of b can be obtained from Eq. 17c. In addition to depending on all the uncertainties that k_r depended on, the uncertainty in b also depends on the uncertainty in X_2 and X_1. As described in the text, X_2 depends on R_b and R_v, whereas X_1 depends on R_v and R_t. The uncertainty in R_v has already been discussed. From the arguments described for the vesicle radius, as well as from measuring the same bead at different times, the uncertainty in the bead radius was taken to be ± 0.3 μm. The error in b also depends on the uncertainty in the tether radius. The expected standard deviation in R_t was calculated by applying the delta method to Eq. 19 in the manuscript. For a vesicle in which the value of R_t ranged from 17 to 23 nm, the expected uncertainty ranged from 0.6 to 1.1 nm. This result was then used to calculate the expected uncertainty in X_1, which was then used to calculated the expected uncertainty in b. The results indicated that the expected deviation in b is quite large, almost 100%, even for a good fit.

CONCLUSION

For the 64 tether pulls, the standard deviation of c_p is 0.007, the standard deviation of k_t is 1.88, and the standard deviation of b is 2.38 (See Fig. 7). Error analysis indicates that even for the same vesicle, the fits to the data are of different quality and can sometimes result in expected deviations larger than those observed. We conclude that the observed distribution in the parameter values is consistent with uncertainties both in measurement and in the parameter values determined by nonlinear regression.

The authors thank Dr. Tony Yeung for discussions on the solution to the diffusion equation and Dr. Dan Hammer for advice on the use of Danckwert's method. The authors also thank Dr. John Kolassa and Ms. Kelly Zou for advice on error propagation analysis of the data presented in Appendix B. The technical assistance of Mr. Richard Bauserman in construction of the probes and microscope improvements and Mrs. Donna Brooks in the bead coating protocol are also gratefully acknowledged.

This work was supported by the U.S. Public Health Service under National Institutes of Health grant HL31524.

REFERENCES

Abramowitz, M., and I. A. Stegun. 1965. Handbook of Mathematical Functions. Dover Publications, New York.

Bevington, P. R. 1969. Data Reduction and Error Analysis for the Physical Sciences. McGraw-Hill, New York.

Bhushan, B., J. Israelachvili, and U. Landman. 1995. Nanotribology: friction, wear and lubrication at the atomic scale. *Nature.* 374:607–616.

Bloom, M., E. A. Evans, and O. Mouritsen. 1991. Physical properties of the fluid lipid-bilayer component of cell membranes: a perspective. *Q. Rev. Biophys.* 24:3:293–397.

Bo, L., and R. E. Waugh. 1989. Determination of bilayer membrane bending stiffness by tether formation from giant, thin-walled vesicles. *Biophys. J.* 55:509–517.

Božič, B., S. Svetina, B. Žekš, and R. E. Waugh. 1992. The role of lamellar membrane structure in tether formation from bilayer vesicles. *Biophys. J.* 61:963–973.

Brumen, M., R. Heinrich, A. Herrmann, and P. Müller. 1993. Mathematical modeling of lipid transbilayer movement in the human erythrocyte plasma membrane. *Eur. Biophys. J.* 22:213–223.

Carslaw, H. S., and J. C. Jaeger. 1959. Conduction of Heat in Solids. Oxford University Press, New York.

Clifford, A. A. 1973. Multivariate Error Analysis. John Wiley and Sons, New York.

Dai, J., and M. P. Sheetz. 1995. Mechanical properties of neuronal growth cone membranes studied by tether formation with laser optical tweezers. *Biophys. J.* 68:988–996.

Danckwerts, P. V. 1951. Absorption by simultaneous diffusion and chemical reaction into particles of various shapes and falling drops. *Trans. Faraday Soc.* 47:1014–1023.

De Kruijff, B., and E. J. J. Van Zoelen. 1978. Effect of the phase transition on the transbilayer movement of dimyristoyl phosphatidylcholine in unilamellar vesicles. *Biochim. Biophys. Acta.* 511:105–115.

De Kruijff, B., E. J. J. Van Zoelen, and L. L. M. Van Deenen. 1978. Glycophorin facilitates the transbilayer movement of phosphatidylcholine in vesicles. *Biochim. Biophys. Acta.* 509:537–542.

Devaux, P. F. 1991. Static and dynamic asymmetry in cell membranes. *Biochemistry.* 30:1163–1173.

Devaux, P. F., and A. Zachowski. 1994. Maintenance and consequences of membrane phospholipid asymmetry. *Chem. Phys. Lipids.* 73:107–120.

Evans, E. A. 1974. Bending resistance and chemically induced moments in membrane bilayers. *Biophys. J.* 16:13–26.

Evans, E. A., and A. Yeung. 1994. Hidden dynamics in rapid changes of bilayer shape. *Chem. Phys. Lipids.* 73:39–56.

Evans, E. A., A. Yeung, R. E. Waugh, and J. Song. 1992. Dynamic coupling and nonlocal curvature elasticity in bilayer membranes. *In* The Structure and Conformation of Amphiphilic Membranes. R. Lipowsky, D. Ritcher, and K. Kremer, editors. Springer-Verlag, Berlin. (*Springer Proc. Phys.* 66:148–153.)

Fourcade, B., L. Miao, M. Rao, M. Wortis, and R. Zia. 1994. Scaling analysis of narrow necks in curvature models of fluid-lipid bilayer vesicles. *Phys. Rev. E.* 49:5276–5286.

Hall, R. N. 1949. The application of non-integral Legendre functions to potential problems. *J. Appl. Phys.* 20:925–931.

Harlow, E., and D. Lane. 1988. Antibodies: A Laboratory Manual. Cold Spring Harbor Laboratory, Cold Spring Harbor, NY.

Heinrich, V., and R. E. Waugh. 1996. A piconewton force transducer and its application to measure the bending stiffness of phospholipid membranes. *Ann. Biomed. Eng.* In press.

Helfrich, W. 1973. Elastic properties of lipid bilayers: theory and possible experiments. *Z. Naturforsch.* 28:693–703.

Hochmuth, R. M., and E. A. Evans. 1982. Extensional flow of erythrocyte membrane from cell body to an elastic tether. I. Analysis. *Biophys. J.* 39:71–81.

Hochmuth, R. M., N. Mohandas, and P. L. Blackshear. 1973. Measurement of the elastic modulus for red cell membrane using a fluid mechanical technique. *Biophys. J.* 13:747–762.

Hochmuth, R. M., J. Shao, J. Dai, and M. P. Sheetz. 1996. Deformation and flow of membrane into tethers extracted from neuronal growth cone. *Biophys. J.* 70:358–369.

Homan, R., and H. J. Pownall. 1987. Effect of pressure on phospholipid translocation in lipid bilayers. *J. Am. Chem. Soc.* 109:4759–4760.

Homan, R., and H. J. Pownall. 1988. Transbilayer diffusion of phospholipids: dependence on headgroup structure and acyl chain length. *Biochim. Biophys. Acta.* 938:155–166.

Kornberg, R., and H. M. McConnell. 1971. Inside-outside transitions of phospholipids in vesicle membranes. *Biochemistry.* 10:1111–1120.

Merkel, R., E. Sackmann, and E. A. Evans. 1989. Molecular friction and epitactic coupling between monolayers in supported bilayers. *J. Phys. France.* 50:1535–1555.

Miao, L., U. Seifert, M. Wortis, and H. G. Döbereiner. 1994. Budding transitions of fluid-bilayer vesicles: the effect of area-difference elasticity. *Phys. Rev. E.* 49:5389–5407.

Needham, D., and E. A. Evans. 1988. Structure and mechanical properties of giant lipid (DMPC) vesicle bilayers from 20° below to 10° above the liquid crystal-crystalline phase transition at 24°C. *Biochemistry.* 27: 8261–8269.

Needham, D., and D. V. Zhelev. 1995. Lysolipid exchange with lipid vesicle membranes. *Ann. Biomed. Eng.* 23:287–298.

Özisik, M. N. 1968. Boundary Value Problems of Heat Conduction. International Textbook Company, Scranton, PA.

Paula, S., A. G. Volkov, A. N. Van Hoek, T. H. Haines, and D. W. Deamer. 1996. Permeation of protons, potassium ions, and small polar molecules through phospholipid bilayers as a function of membrane thickness. *Biophys. J.* 70:339–348.

Reeves, J., and R. Dowben. 1969. Formation and properties of thin-walled phospholipid vesicles. *J. Cell Physiol.* 73:49–60.

Rothman, J., and E. Dawidowicz. 1975. Asymmetric exchange of vesicle phospholipids catalyzed by the phosphatidylcholine exchange protein. Measurement of inside-outside transitions. *Biochemistry.* 14: 2809–2816.

Seifert, U., K. Berndl, and R. Lipowsky. 1991. Shape transformations of vesicles: phase diagram for spontaneous-curvature and bilayer-coupling models. *Phys. Rev. A.* 44:1182–1202.

Sheetz, M. P., and S. J. Singer. 1974. Biological membranes as bilayer couples. A molecular mechanism of drug-erythrocyte interactions. *Proc. Natl. Acad. Sci. USA.* 71:4457–4461.

Svetina, S., and B. Žekš. 1989. Membrane bending energy and shape determination of phospholipid vesicles and red blood cells. *Eur. Biophys. J.* 17:101–111.

Vaz, W., Z. Derzko, and K. Jacobson. 1982. Photobleaching measurements of the lateral diffusion of lipids and proteins in artificial phospholipid bilayer membranes. *In* Membrane Reconstitution. G. Poste and G. L. Nicolson, editors. Elsevier Biomedical Press, Amsterdam, the Netherlands. 83–136.

Waugh, R. E., and R. Bauserman. 1995. Physical measurements of bilayer-skeletal separation forces. *Ann. Biomed. Eng.* 23:308–321.

Waugh, R. E., J. Song, S. Svetina, and B. Žekš. 1992. Local and nonlocal curvature elasticity in bilayer membranes by tether formation from lecithin vesicles. *Biophys. J.* 61:974–982.

Wimley, W. C., and T. E. Thompson. 1990. Exchange and flip-flop of dimyristoylphosphatidyl-choline in liquid-crystalline, gel and two-component, two-phase large unilamellar vesicles. *Biochemistry.* 29: 1296–1303.

Wimley, W. C., and T. E. Thompson. 1991. Transbilayer and interbilayer phospholipid exchange in dimyristoylphosphatidylcholine/dimyristoylphosphatidylethanolamine large unilamellar vesicles. *Biochemistry.* 30:1702–1709.

Wu, E., K. Jacobson, and D. Papahadjopoulos. 1977. Lateral diffusion in phospholipid multibilayers measured by fluorescence recovery after photobleaching. *Biochemistry.* 16:3936–3942.

Yeagle, P. 1993. The Membranes of Cells, 2nd Ed. Academic Press, San Diego.

Yeung, A. 1994. Mechanics of inter-monolayer coupling in fluid surfactant bilayers. Ph.D. thesis. Department of Physics, University of British Columbia, Vancouver, B.C., Canada.

Yoshizawa, H., Y. Chen, and J. Israelachvili. 1993. Fundamental mechanisms of interfacial friction. 1. Relation between adhesion and friction. *J. Phys. Chem.* 97:4128–4140.

Yoshizawa, H., and J. Israelachvili. 1994. Relation between adhesion and friction forces across thin films. *Thin Solid Films.* 246:71–76.

Zachowski, A. 1993. Phospholipids in animal eukaryotic membranes: transverse asymmetry and movement. *Biochem. J.* 294:1–14.